

Topological reciprocity in 3D superconducting diodes

Philip Moll

philip.moll@mpsd.mpg.de

Max Planck Institute for the Structure and Dynamics of Matter <https://orcid.org/0000-0002-7616-5886>

Article

Keywords:

Posted Date: April 10th, 2024

DOI: <https://doi.org/10.21203/rs.3.rs-4050345/v1>

License:  This work is licensed under a Creative Commons Attribution 4.0 International License.

[Read Full License](#)

Additional Declarations: There is **NO** Competing Interest.

Topological reciprocity in 3D superconducting diodes

Philip JW Moll

Max-Planck-Institute for Structure and Dynamics of Matter, Hamburg, Germany

Philip.moll@mpsd.mpg.de

The design of advanced functionality in superconducting devices usually focuses on materials engineering, either in heterostructures or in compounds of unconventional quantum materials. Here we demonstrate a different strategy to bespoke behavior by controlling the 3D shape of superconductors on the micron-scale. As a demonstration, a large superconducting diode effect is engineered solely by 3D shape design of a conventional superconductor, ion-beam deposited tungsten. Its highly efficient diode behavior appears from its triangular cross-section when vortices break time-reversal and all mirror symmetries. Yet reciprocity is observed at special field angles where the lack of symmetry would lead one to expect diode behavior. This can be understood as a topological mechanism that is robust against deformations of the triangle. Geometry and topology induce a rich internal structure due to the high-dimensional tuning parameter space of 3D structures, inaccessible to the conventional 2D design strategies in thin films.

Currently superconducting electronics rise in attention of the research community as quantum information processing on superconducting platforms is looming on the horizon. With quantum coherence as the new benchmark of circuit design, their unique characteristics as macroscopically coherent systems may finally overcome the economical challenges of their cryogenic temperature requirements. When such qubits set (ultra-)low operation temperatures, exciting new opportunities even for classical superconducting circuit elements follow. In particular, the superconducting diode currently receives significant attention due to novel mechanisms of non-reciprocal charge transport compared to classical, single-electron electronics.

Superconductors support lossless dc-current flow up to its critical current, I_c , above which resistance and dissipation set in. In a superconducting diode, the critical current magnitude depends on the current polarity, $I_c^+ \neq I_c^-$. Such a device would offer ideal current rectification and direct signal propagation in superconducting electronics similar to diodes in ambient electronics. Fundamentally, superconductors that simultaneously break time-reversal and mirror symmetries may differentiate between forward and backward currents. Theory predicts these symmetry conditions in the bulk of exotic superconductors, for example in finite momentum pairing systems¹⁻³ or chiral SC that inherently break time-reversal symmetry⁴. Experimental observations have been reported in non-centrosymmetric crystals, such as the Dirac semi-metal NiTe₂ (ref.⁵), twisted trilayer graphene⁶, or heterostructures with varying spin-orbit coupling⁷.

While here non-reciprocity heralds new insights into exotic superconducting states, their diode efficiency is typically too low for practical applications. The efficiency is quantified as the normalized difference between the magnitude of the critical currents, $\eta = \frac{I_c^+ - I_c^-}{I_c^+ + I_c^-}$, ranging from zero (reciprocal transport) to one (ideal rectification). Here, vortex matter offers an established and optimized platform for the design of high-efficiency diodes under an external magnetic field. When the macroscopic shape of the superconductor breaks the mirror symmetry along the channel and vortices break time-reversal symmetry, non-reciprocity is the norm and diode behavior has been routinely observed for decades⁸⁻¹⁰. In this context, the term “asymmetric critical current” is used to denote SC diode behavior. Vortex entry and exit is highly dependent on the microscopic details of the surface barrier, such that minute and almost unavoidable fabrication imperfections suffice for diode behavior^{11,12}. Thin-film devices with engineered asymmetry show sizable diode effects, for example due to engineered boundary

asymmetry, asymmetric anti-dot arrays¹³, superconductor/ferromagnet bilayers¹¹, as well as Josephson junctions with individual trapped vortices¹⁴. The engineering challenge towards ideal vortex diodes thus is to create maximally left-right asymmetric channels, and to tailor the non-linearity to match the requirements of real applications.

The physics of vortices and associated non-reciprocity is well established in thin-film (2D) and bulk (3D) geometries^{15–20}. Here we report an alternative regime of superconductors on a scale of comparable to multiple penetration depths that are meaningfully three-dimensional. This denotes micron-sized wires with cross-section geometries that clearly differ from simple extrusions and thus truly are 3D objects. This concept is demonstrated in the specific case of a wire with a triangular cross-section, yet extensions to other geometric shapes naturally expand to further phenomena. Related triangular rods, hand-polished on the mm-scale, have already in 1965 been demonstrated by Swartz and Hart⁸ to be excellent SC diodes, albeit operating in a different physical regime of surface current flow owing to their macroscopic size and bulk pinning impeding vortex motion. Utilizing state-of-the-art microfabrication, controlling the cross-section shape becomes a higher-dimensional tuning parameter for vortex matter, and concepts from geometry and topology naturally enter their physics as is here demonstrated in the triangular superconducting diode.

For a vortex system to be dominated by the 3D shape of the superconductor, the dominant force acting on vortices should be the energy barrier associated with their entry and exit, the Bean-Livingston barrier²¹. Akin to mirror charges in electrostatics, the surface provides a repulsive force hindering vortices from crossing it. Commonly, however, bulk defect pinning provides the dominant force in 3D objects²². Local defects suppress the condensation energy, which define lower energy positions of vortices and thus impede their free motion and the associated dissipative voltage. Bulk pinning can either be minimized in ultra-clean crystals, or in ultra-disordered systems in which a high defect density compared to the vortex diameter effectively averages the pinning potential. We focus here on the recent observations of ultra-mobile vortices in Focused Ion Beam deposited superconductors^{23–25}. W-C-O is a highly carbon-rich amorphous superconducting deposit of tungsten²⁶. It features a decent $T_c \sim 5K$ and upper critical field $H_{c2}(0K) \sim 9.5T$, and accordingly one obtains the Ginzburg-Landau coherence length $\xi(0K) \sim 6nm$. The penetration depth is more difficult to infer in microstructures, yet using standard estimates from transport $\lambda(0K) \sim 650nm$ has been reported²⁷. This high penetration depth arises from the high normal state resistivity and is in line with the limited mean-free-path in this amorphous material. Tunneling spectroscopy²⁸ unveils a fully gapped state with $\Delta(0K) = 0.65meV$, and a consistent picture of a conventional, strongly type-II superconductor deep in the dirty limit emerges.

This material can be conveniently deposited in a maskless direct-write technique on any substrate which allows non-trivial shape control in 3D (see supplement for fabrication details). Here we focus on a $10\mu m$ long wire with a cross-section precisely shaped as an oblate isosceles triangle ($2.8\mu m$ wide, $7.0\mu m$ tall, Fig. 1). The amorphous nature of the deposits is evidenced by the approximately temperature-independent resistance, placing them close to a metal-insulator transition. The SC transition, however, is sharp and a noise-limited zero-resistance state is reached. We note a weak double-transition in the cooldown which follows from slightly different T_c in the current injection contacts compared to the wire itself (see methods). To avoid complications of Lorentz-force modulations or pinning effects at the contacts, we strictly keep the magnetic field perpendicular to the wire while rotating. The field-angle θ parametrizes the field direction, where $\theta = 0^\circ$ corresponds to fields aligned with the tip of the triangle (Fig. 1).

When dominated by surface barrier pinning, such an object naturally acts as a highly efficient superconducting diode (Fig. 2), and the single current-polarity conserving mirror plane of the geometric object plays a crucial role. When the magnetic field is applied within this mirror plane, that is $\theta = 0^\circ$, symmetry dictates an entirely anti-symmetric current-voltage characteristics (IV-curve) as

experimentally observed (black curve). Careful checks for self-heating have been performed such that in the presented current range overdriving and thermal effects are negligible. As the field is rotated out of this plane, the vortices explicitly and strongly break the mirror symmetry. Hence within a narrow angle range a massively asymmetric diode behavior emerges. This asymmetry finds a maximum at $\theta = 11^\circ$, which corresponds to half of the geometric opening angle of the isosceles triangle studied here, 22° . Here the field is parallel to the left sidewall, which is a maximally asymmetric configuration of vortices entering either through a steep wall on one or through the knife-edge geometry on the other side. A large diode effect results as the current polarity sets the direction of the Lorentz force, $F_L \propto j_s \times B$, and vortex velocity perpendicular to the channel, and thereby which physical edge vortices have to enter. Moving to $\theta = -11^\circ$ aligns the field parallel with the opposite side, which inverts the diode from forward to backward. It is gratifying to see the nearly perfect asymmetry between these two directions, which evidences highly similar surface barriers on both faces as desired, which in turn demonstrates the achieved fabrication quality and reproducibility in this 3D structure. These results clearly demonstrate that vastly asymmetric vortex barriers, and hence SC diodes, can be achieved with 3D shape control deterministically. Unlike thin-films in 2D, the field direction plays a crucial role which does not only set the magnitude but also the forward direction of the diode. It follows naturally that the diode strength and field angle behavior can be designed as desired by changing the triangle shape. This sets such systems apart from engineered surface asymmetries in 2D, which are only sensitive to the out-of-plane component of the field when orbital effects are considered. Accordingly, in any 2D diode design a field polarity change (or 180° rotation) is necessary to reverse the forward direction at given current polarity. Control over arbitrary field angles for the diode strength and polarity reversal within a small angle range are new features uniquely enabled by the 3D nature of these devices.

Another important distinction of 3D bulk-like superconductors, as compared to thin films, is the sustainable flux-flow without discrete avalanching or a thermal runaway induced transition into the normal state. The here reported IVs merge smoothly into a zero-voltage state, and thus are not necessarily characterized by a sharp critical current. It is instead useful to define a critical voltage, either given by experimental resolution or concrete application demands, that implicitly defines a critical current as $V(I_c) = V_c$. For an initial glimpse at the data, one may trace the critical currents and the nominal η as a rough measure of the diode strength over a full field rotation (Fig. 2b,c, $V_c = 1\mu V$). Beyond the rapid increase of η up to 11° , a broad region of smoothly weakening diode strength follows. Eventually at 90° , η changes sign as now the field is parallel to the short bottom face of the triangle. Due to the high symmetries of the problem, one quadrant (0° - 90°) fully characterizes the device. Time-reversal symmetry ensures $V(I, B) = V(-I, -B) \equiv V(-I, \theta + 180^\circ)$, hence $\eta(\theta) = -\eta(\theta + 180^\circ)$. Equally, the mirror symmetry enforces $\eta(\theta) = -\eta(-\theta)$, leading to symmetry-protected reciprocal transport ($\eta = 0$) for fields in the mirror plane, $\theta = 0^\circ, 180^\circ$.

Six zero-crossings of η are observed over the full circle, and each of these zero crossings correspond to a configuration of reciprocal transport, four more than required by symmetry in this geometry. At any oblique field angle this symmetry is explicitly broken, thus nonreciprocity is allowed and indeed observed at all angles— except for the additional zero crossing at $\theta_{top} \sim 72^\circ$ (and its symmetry-related copies). This apparently accidental degeneracy is even more surprising given the large number of degrees of freedom that parametrize the non-linear IV-curves, which requires a discussion beyond a simple number η . Its value depends on an arbitrary voltage criterion and thus has little merit in assessing neither the physical situation nor the technical relevance of the diode for a certain application. For example, carefully adjusting the experimental parameters and V_c would, close to T_c , technically allow us to report record numbers of η well above 90% with little physical meaning.

To better appreciate the non-reciprocity in these devices, we thus focus on the raw IV curves as customary in semiconducting diodes. Perfectly reciprocal conductance reflects in anti-symmetric IV

curves, as $V(I) = -V(-I)$. Hence the symmetric voltage, $V_{sym} = \frac{1}{2}(V(I) + V(-I))$, is a more nuanced measure that directly encodes the diode strength at a current level I .

The angle dependence of V_{sym} further highlights the surprising robustness of reciprocity at θ_{top} (Fig.3), as the IV curve is highly symmetric over the entire current range. Equivalently, the efficiencies defined at any voltage criteria, $\eta(\theta, V_c)$, cross zero at the angle θ_{top} . While it is a natural consequence of continuity of a sign-changing real function $\eta(\theta)$ to cross zero somewhere, one would not expect to tune a complex curve $V_{sym}(I)$ to zero with a single parameter. In the case of the symmetry-protected zero-crossings of η , this is enforced by conservation laws arising from time-reversal and mirror symmetry. At the oblique angle θ_{top} , no symmetry argument can be made and reciprocity appears merely accidental. We note that V_{sym} does not vanish exactly at θ_{top} , with a similar residual magnitude compared to that in the symmetric orientation $\theta = 0^\circ$. This small residual signal points to experimental deviations from the idealized case, such as non-ideal triangular shapes, thermal effects from weak but asymmetric self-heating or field precession due to slight deviations of the triangular wire from the axis of rotation. Nonetheless, the data clearly shows that a notable degree of reciprocity at the low-symmetry configuration θ_{top} .

There are two mechanisms that protect degeneracies in physical systems, symmetry and topology. Symmetry produces exact relations, which here force even terms in the IV-curve to vanish. In topology, objects are classified by invariants that are stable against smooth deformations. Unlike symmetry, they do not constrain exact locations of degeneracies but rather enforce their existence somewhere as seen for example in the low-symmetry location of Weyl nodes in k-space in topological electronic band structures. Here, we argue that the reciprocity at θ_{top} is based on topology, and generic to superconductors of triangular cross-section. η is bound to exhibit six extrema alternating between minima and maxima in one full revolution. Due to time-reversal symmetry, these extrema are bound in pairs of one minimum and one maximum, separated by a half-rotation. As a result, it must always exhibit six zeros, and symmetries may further constrain their location on the circle. This is generic to arbitrary triangles, and in that sense the number of vertices of the triangle ($n = 3$) takes the role of a topological invariant. Any smooth deformation of the cross-section within the space of triangles may only move the zeros, but not remove them.

To understand the geometric structure of the nonreciprocity from a vortex point-of-view, we first point to the importance of the special configurations when the magnetic field is parallel to one of the three faces of the triangle (Fig. 4). In the absence of bulk pinning, the well-controlled 3D shape results in a geometric force acting on the vortices. The flux lines are expected to follow the direction of the magnetic field given the microscopic wire geometry and hence the absence of notable demagnetization effects. Assuming straight vortices, their length depends linearly on the position within the triangle. This causes a position dependent potential energy of the vortex $U(x) = \alpha \epsilon x$, given a constant line energy ϵ per unit length and $\alpha = \frac{dl}{dx}$ denoting the geometric length change of the vortex. From this argument, a purely geometric force results, $F_{geom} = -\alpha(x)\epsilon$, which acts in addition to the Lorentz force F_L on the vortices.

Any triangle decays into two regions of opposite sign of this geometric force (orange and yellow in Fig.4a). These regions evolve as the triangle rotates in the magnetic field. As the vortex lines follow the magnetic field, α is tuned by the field angle. Importantly, α and thus the geometric force diverges at the special angles when the field is parallel to a triangle face, providing the highest barrier for vortex penetration. This picture is well supported by the angle-dependence of $I_c(\theta)$, which shows pronounced spikes and sharp I_c maxima at these geometric angles. In addition to an enhanced overall I_c , also a

maximum in the diode effect is expected as observed reflecting the maximal left-right asymmetry for vortices.

The sixfold alternation of the diode sign reveals an interesting geometric hierarchy of generic IV-curves in triangular conductors. In the most symmetric case of an equilateral triangle, each of its three mirror planes pins two crossings at multiples of 60° , $\theta = i 60^\circ, i = \{0,1, \dots 5\}$ and symmetry exactly explains all reciprocal angles. Deforming the triangle into an isosceles one breaks two mirrors yet the left-right alternation still enforces six reciprocal directions. Hence the four zero crossings associated with the broken symmetries cannot be removed but may now slide on the circle away from the multiples of 60° . Further deforming the triangle to a general scalene one breaks all mirror symmetries, in which case all zero-crossings may fall on arbitrary angles yet are still protected by topology. As any triangle can be smoothly deformed into an equilateral one without leaving the space of triangles, these reciprocal topological angles are remnants of the higher symmetry in the equilateral triangle.

The overall flower-shaped $\eta(\theta)$ can be well captured by a simple geometric model based on the shape of the triangle alone, supporting the notion that the geometric surface barrier dominates over bulk pinning (see supplement). While clearly microscopic modeling is required to explain the details of the nonreciprocity, the success of this outrageously oversimplified model further supports that geometry is the key factor in the device response. By design, the model predicts a zero crossing at the mirror-symmetry enforced angles, yet it clearly fails to predict the location of the topological reciprocity which further supports that it has no geometric meaning in the triangle. This is also experimentally supported by the field and temperature-dependence of the topological angle (Fig. 4d) which varies substantially from 77° at (80mT,4K) to 50° at (40mT, 3K), while the symmetry-enforced degeneracies are constant within experimental resolution of the angle ($\pm 0.2^\circ$). Temperature tunes the vortex size and interaction, while the magnetic field sets their density. This not surprisingly impacts the non-linearity of conduction and thereby the IV curves. While these details move the location of the topological reciprocity, they do not lift this degeneracy.

Arguments based on geometry, symmetry and topology suffice to capture the geometric properties of transport reciprocity and expose the underlying structure. In real materials, the topological arguments will naturally fail at the boundary of triangle space, such as when the triangle is deformed into a thin film by reducing one leg to zero or its cross-section is shrunk towards a nanowire. Further these considerations do not allow to model the IV curves or even the angular dependence of η , as microscopic ab-initio models are necessary to provide this. Time-dependent Ginzburg-Landau simulations in 3D mesoscopic structures are challenging yet present a straightforward pathway to the rational design of superconducting diodes with fine-tuned IV-characteristics.

In combination, these results clearly demonstrate that non-trivial 3D geometries open a rich door for engineering of advanced electronic functionality even in traditional superconductors. Importantly, the 3D cross-section is a powerful yet thus-far neglected tuning space. The most studied platforms of thin (2D) or thick planar films (rectangular cross-section) are of too high symmetry to exhibit non-trivial shapes. For example, the inversion symmetry in rectangular conductors as the most simple 3D shape does not support non-reciprocity at any field angle. With more complex 3D designs, diodes with bespoke field-angle response and desired current-voltage characteristics can be fabricated. In particular, the forward direction can be flipped by a small field-angle change, in stark contrast to the field polarity change required in 2D geometries. With 3D control providing a higher-dimensional geometric tuning space for these systems, non-trivial forms of topology emerge such as the topologically protected reciprocity within the space of triangles reported here.

This observation provides a promising starting point for explorations of other shapes and topological transitions in search for new function, such as a pentagon or irregular polygon. At the same time, a

convergence of the counterintuitive robustness of the degeneracy with microscopic models is needed to fully appreciate the topologically protected reciprocity. It will be very interesting to explore which other complex interacting systems can be imprinted with topology via precise geometric control, given they can be made clean enough such that their physical shape dominates their behavior. Clearly, geometric sources of topology in interacting systems deserve closer investigation.

Acknowledgements: This project was supported by the ERC action XBEND. PJWM is grateful for inspiring discussions with Titus Neupert, Mark Fischer, Vadim Geshkenbein, Alexander Balatsky, and greatly appreciates the mqm team at MPSD for their tolerance and support of occasional PI experiments in the lab, especially Carsten Putzke and Chunyu Guo. Kaize Wang parametrized the area variation with angle. Thanks!

References

1. Yuan, N. F. Q. & Fu, L. Supercurrent diode effect and finite-momentum superconductors. *Proc. Natl. Acad. Sci. U. S. A.* **119**, 1–7 (2022).
2. He, J. J., Tanaka, Y. & Nagaosa, N. A phenomenological theory of superconductor diodes. *New J. Phys.* **24**, (2022).
3. Daido, A., Ikeda, Y. & Yanase, Y. Intrinsic Superconducting Diode Effect. *Phys. Rev. Lett.* **128**, 37001 (2022).
4. Zinkl, B., Hamamoto, K. & Sigrist, M. Symmetry conditions for the superconducting diode effect in chiral superconductors. *Phys. Rev. Res.* **4**, 1–12 (2022).
5. Pal, B. *et al.* Josephson diode effect from Cooper pair momentum in a topological semimetal. *Nat. Phys.* **18**, 1228–1233 (2022).
6. Lin, J. X. *et al.* Zero-field superconducting diode effect in small-twist-angle trilayer graphene. *Nat. Phys.* **18**, 1221–1227 (2022).
7. Ando, F. *et al.* Observation of superconducting diode effect. *Nature* **584**, 373–376 (2020).
8. Swartz, P. S. & Hart, H. R. Surface effects in the mixed superconducting state. *Phys. Rev.* **137**, (1965).
9. Owen, C. S. & Scalapino, D. J. Vortex structure and critical currents in Josephson junctions. *Phys. Rev.* **164**, 538–544 (1967).
10. Morrison, D. & Rose, R. CONTROLLED PINNING IN SUPERCONDUCTING FOILS BY SURFACE MICROGROOVES. *Phys. Rev. Lett.* **25**, 356 (1970).
11. Hou, Y. *et al.* Ubiquitous Superconducting Diode Effect in Superconductor Thin Films. *Phys. Rev. Lett.* **131**, 027001 (2023).
12. Plourde, B. L. T. *et al.* Influence of edge barriers on vortex dynamics in thin weak-pinning superconducting strips. *Phys. Rev. B* **64**, 014503 (2001).
13. Lyu, Y. Y. *et al.* Superconducting diode effect via conformal-mapped nanoholes. *Nat. Commun.* **12**, 2703 (2021).
14. Golod, T. & Krasnov, V. M. Demonstration of a superconducting diode-with-memory, operational at zero magnetic field with switchable nonreciprocity. *Nat. Commun.* **13**, 3658 (2022).

15. Aliev, F. G. Generation of DC electric fields due to vortex rectification in superconducting films. *Phys. C Supercond. its Appl.* **437–438**, 1–6 (2006).
16. Chahid, S., Teknowijoyo, S., Mowgood, I. & Gulian, A. High-frequency diode effect in superconducting Nb₃Sn microbridges. *Phys. Rev. B* **107**, 1–8 (2023).
17. Vodolazov, D. Y. & Peeters, F. M. Superconducting rectifier based on the asymmetric surface barrier effect. *Phys. Rev. B* **72**, 172508 (2005).
18. Wambaugh, J. F., Reichhardt, C., Olson, C. J., Marchesoni, F. & Nori, F. Superconducting fluxon pumps and lenses. *Phys. Rev. Lett.* **83**, 5106–5109 (1999).
19. Jin, B. B. *et al.* High-frequency vortex ratchet effect in a superconducting film with a nanoengineered array of asymmetric pinning sites. *Phys. Rev. B* **81**, 1–7 (2010).
20. Togawa, Y. *et al.* Direct observation of rectified motion of vortices in a niobium superconductor. *Phys. Rev. Lett.* **95**, 1–4 (2005).
21. Bean, C. P. & Livingston, J. D. Surface barrier in type-II superconductors. *Phys. Rev. Lett.* **12**, 14–16 (1964).
22. Blatter, G., Feigel'man, M., Geshkenbein, V., Larkin, A. & Vinokur, V. Vortices in high-temperature superconductors. *Rev. Mod. Phys.* **66**, 1125–1387 (1994).
23. Dobrovolskiy, O. V. *et al.* Ultra-fast vortex motion in a direct-write Nb-C superconductor. *Nat. Commun.* **11**, 3291 (2020).
24. Córdoba, R. *et al.* Long-range vortex transfer in superconducting nanowires. *Sci. Rep.* **9**, 1–10 (2019).
25. Guillamón, I. *et al.* Direct observation of melting in a two-dimensional superconducting vortex lattice. *Nat. Phys.* **5**, 651–655 (2009).
26. Sadki, E. S., Ooi, S. & Hirata, K. Focused-ion-beam-induced deposition of superconducting nanowires. *Appl. Phys. Lett.* **85**, 6206–6208 (2004).
27. Córdoba, R. *et al.* Magnetic field-induced dissipation-free state in superconducting nanostructures. *Nat. Commun.* **4**, 1437 (2013).
28. Guillamón, I. *et al.* Nanoscale superconducting properties of amorphous W-based deposits grown with a focused-ion-beam. *New J. Phys.* **10**, (2008).

Figures

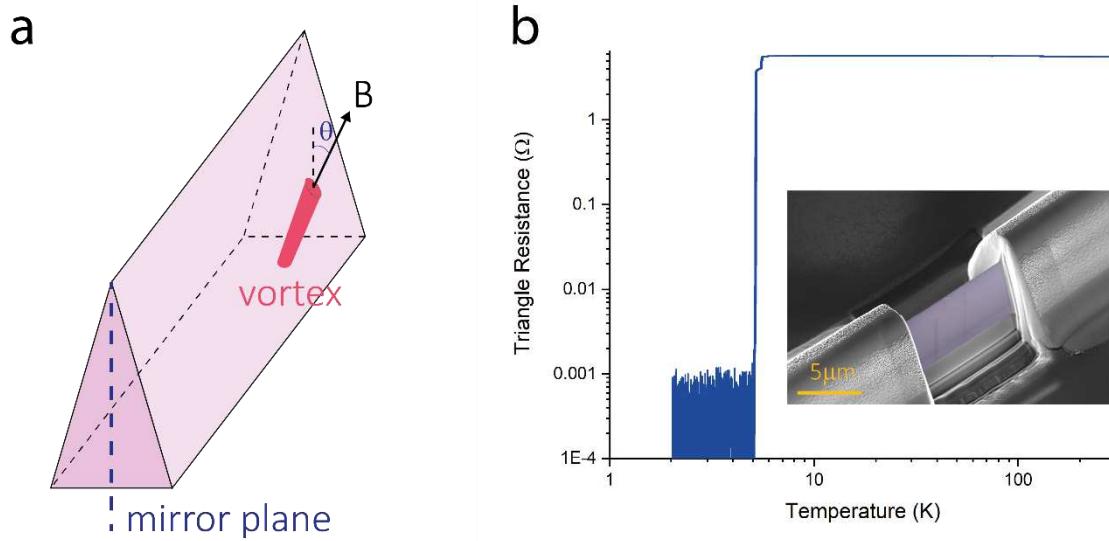


Fig. 1 Triangular mesoscopic superconductor. A) the active device is a straight wire with an isosceles triangular cross-section. Importantly, this shape features only one mirror symmetry that preserves the current polarity. The magnetic field angle, θ , sets the direction of vortices and is measured from that mirror plane. B) Inset: False-color SEM image of the real wire. The $10 \mu\text{m}$ long active section (purple) terminates in much bigger, bulky superconducting terminals to ensure the smallest critical current takes place in the triangular section. The isosceles triangle is $2.8 \mu\text{m}$ wide and $7.0 \mu\text{m}$ tall, corresponding to an opening angle of 22° . Main: The resistance remains essentially independent down to $T_c = 5.25$ K. A weak double-transition appears due to a slightly higher T_c in the large SC contacts that were deposited at higher ion currents.

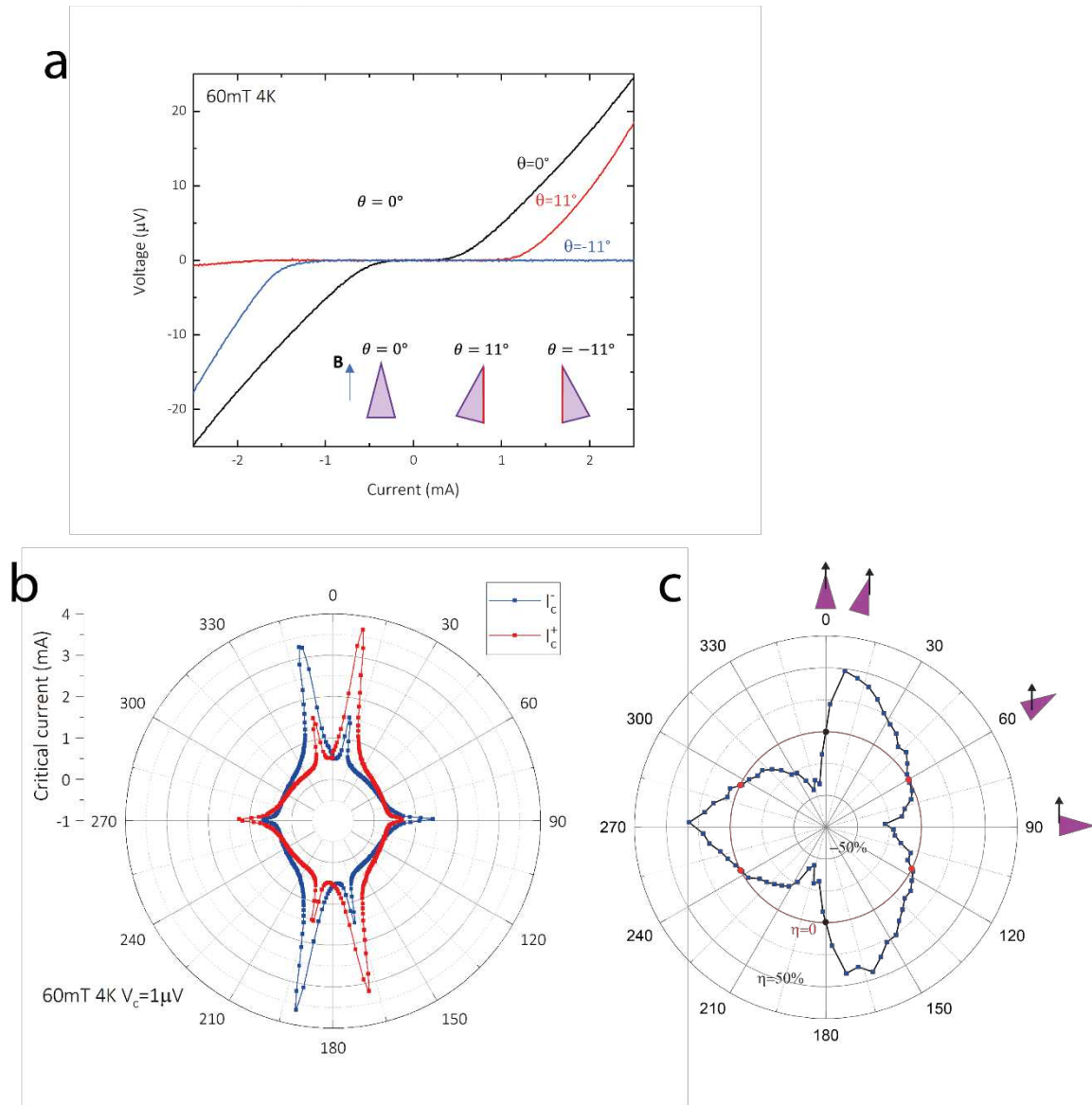


Fig. 2: Superconducting vortex diode. a) The current-voltage characteristics in the symmetric configuration ($\theta = 0^\circ$) is highly anti-symmetric while at shallow angles ($\pm 11^\circ$) pronounced diode effects are observed. In line with symmetry, the diode forward direction flips when rotating through $\theta = 0^\circ$. b) Over a full field rotation, the critical current is strongly modulated. The mirror symmetric appearance of I_c^+ and I_c^- reflects how close the device is to the idealized triangle. Strong peaks occur at 6 angles with pronounced diode behavior. These correspond to special angles when the magnetic field is parallel to one of the triangle faces. c) The diode efficiency η computed at a voltage criterion $V_c = 1\mu V$ displays a distinct flower-shape associated with the triangle geometry. η crosses zero (red circle) at 6 angles, two at the mirror symmetric directions $0^\circ, 180^\circ$ and 4 times at low symmetry directions θ_{top} (and its symmetry copies).

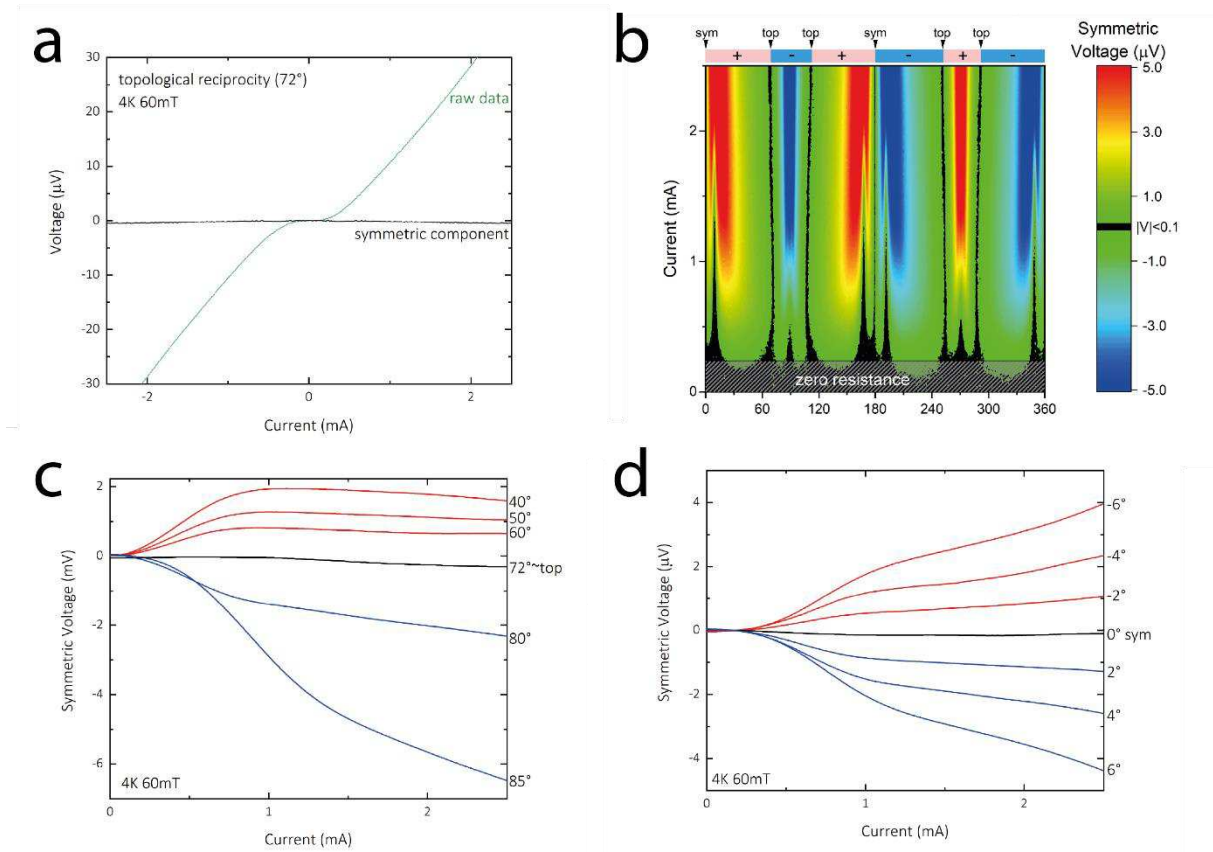


Fig. 3 Symmetry and topology. a) IV curve at the topological angle $\theta_{top} \sim 72^\circ$ (@4K, 60mT) is highly anti-symmetric over the entire current range, despite the lack of symmetry at this angle. The symmetric component V_{sym} is flat accordingly. b) Scanning IV curves at same conditions in 1° steps exposes the angular structure of V_{sym} . The diode direction changes six times over a full revolution, with reciprocal cases found equivalently six times (black lines, $V_{sym} = 0$). c) and d) highlight the angular evolution of V_{sym} (@4K, 60mT) crossing through the topological and symmetry-governed reciprocal angles. We associate the subtle deviations of V_{sym} from zero at both angles with deviations of the real device from the idealized geometry.

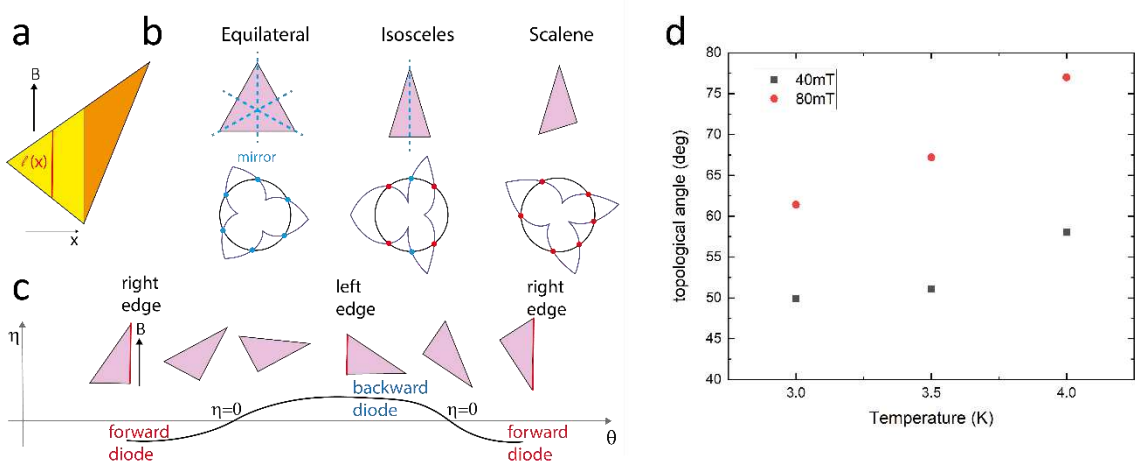


Fig. 4 Evolution of topology. a) The triangular cross-section renders the length of the vortices following the field direction position dependent, $l(x)$, which forms the basis of the geometric force. At any angle except for the critical ones, the triangles decay into two regions (yellow and orange) with F_{geom} of

different magnitude and opposite direction. b) Each mirror symmetry constrains a pair of zero crossings. While the equilateral triangle pins all six crossings at mirror symmetry protected angles (blue dot), in the isosceles only two are set by symmetry, and in the scalene case all six crossings fall into the topological category (red dot). Exemplary plots of $\eta(\theta)$ are sketched, using the model presented in the supplement. c) The alternating left-right asymmetry is a natural consequence of any triangle, irrespective of its symmetries. d) The topological angle is strongly field and temperature dependent, reflecting its decoupling from geometry.

Supplement

S1: Fabrication details

The tungsten deposition was performed in a Ga-based focused ion beam (ThermoFisher Helios G4). The standard precursor gas $W(CO)_6$ was introduced to the chamber via the micro-nozzle of the ThermoFisher gas injection system. The substrate is a sapphire chip with photolithographically patterned gold leads. The leads were grounded for effective charge removal during the charged beam operation. Optimal deposition conditions were found at 12kV beam energy and 50ns dwell time. A seed layer of $\sim 10\text{nm}$ was deposited at low currents of 0.3nA to avoid distortions of the structure due to charging effects. Once the seed layer robustly connected to the electrodes, a clear discharge and sharp, well grounded image appeared. For the growth of the entire structure, a high current of 20nA was used to grow a $100\mu\text{m}$ long, $5\mu\text{m}$ wide and $7\mu\text{m}$ tall rectangular deposit. In addition, side contacts that serve as four-probe voltage measurements were grown connecting further gold pads to a $10\mu\text{m}$ long section in the center of the wire, that would later become the triangular wire. These connecting wires were grown at 45nA to accelerate the deposition, and as the superconducting parameters are known to be beam condition dependent, now show a slightly different T_c yielding the weak double-step appearance in main Fig. 1.

The triangular wire was then FIB cut into the center section. The chip surface in this machine is normal to the ion beam at 52° . To achieve an opening angle of 20° for the isosceles triangle, the stage was tilted to 42° and polished using 300pA at 30kV. The targeted opening angle of 20° is in very good agreement with the experimentally determined opening angle of 22° from magnetotransport, with a slight increase due to the finite width of the beam and the opening angle of the cut.

S2: Geometric model

The full dynamics of the driven vortex system requires a 3D simulation of the time-dependent Ginzburg-Landau model. This is complicated by the mesoscopic shape of the triangle (size $\sim 10 - 100\lambda$) and the non-negligible role of the geometric boundary. These challenging calculations will be an important step towards unlocking the engineering potential of 3D vortex matter. At the same time, it is gratifying to see how far arguments purely based on geometry, topology and symmetry go in explaining the complex data. These arguments can only yield, however, understanding at and closely around specific angles such as θ_{top} .

Here we work out a geometric model to elucidate to what surprising degree the anisotropy over a full angle rotation can be understood based on geometry alone. The model is phenomenological, and microscopic simulations are necessary to fill in the details. In particular, the model fails to predict the location of the topological angle. This further reinforces the fact that its location is not based on geometry, which echoes in its temperature- and field-dependent value.

To capture the triangle geometry, one may be tempted to use the ratio of the geometric forces. Any triangle at arbitrary field angle decays into two regions in which the geometric force takes a different value with opposite direction. It is a straightforward geometric exercise to compute these two areas A_{right} and A_{left} . The scaled difference between these areas $\tilde{\eta} = c (A_{left} - A_{right}) / (A_{left} + A_{right})$ is a natural proxy for the degree of imbalance between the forces. It obeys all symmetry requirements, for example, in the isosceles triangle $\tilde{\eta}$ vanishes by design at the mirror symmetric configuration $\theta = 0^\circ$ as both areas are equal.

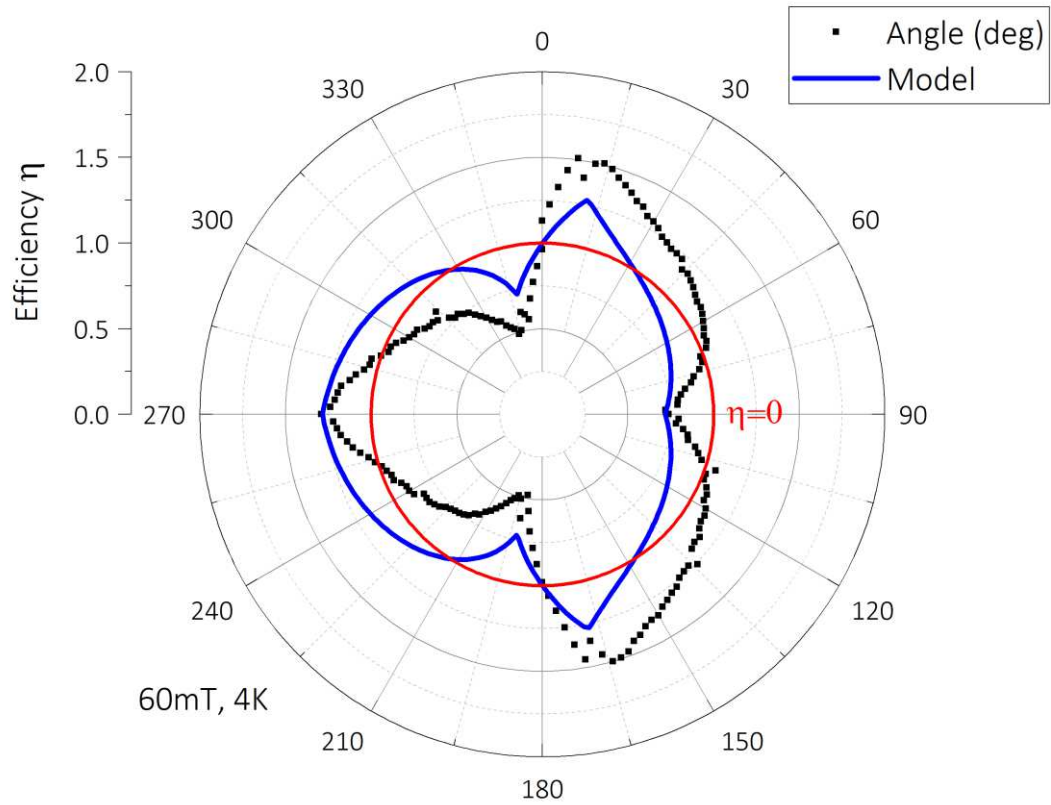


Fig. S2.1: Comparison of the geometric model to the measured $\eta(1\mu V)$ at 60mT, 4K.

This geometric construction reproduces the overall flower-shape remarkably well, supporting that the surface boundary following the geometry is the dominant factor setting the non-reciprocity.